COROTATIONAL VELOCITY STRAIN FORMULATIONS FOR NONLINEAR ANALYSIS OF BEAMS AND AXISYMMETRIC SHELLS*

Ted Belytschko
Department of Civil Engineering
Northwestern University, Evanston, Illinois

H. Stolarski
Institute of Fundamental Technological Research
Polish Academy of Sciences, Warsaw, Poland

C.S. Tsay
Northwestern University

SUMMARY

Finite element formulations for large strain, large displacement problems are formulated using a kinematic description based on the corotational components of the velocity strain. The corotational components are defined in terms of a system that rotates with each element and approximates the rotation of the material. To account for rotations of the material relative to this element system, extra terms are introduced in the velocity strain equations. Although this formulation is incremental, in explicitly integrated transient problems it compares very well with formulations that are not. Its simplicity, and its compatibility with constitutive equations found in "hydro" codes make it very attractive for this class of problems.

INTRODUCTION

Nonlinear structures are conventionally treated by kinematic descriptions that are essentially Lagrangian in nature, in that the measure of deformation is directly related to the total displacements. Several types of Lagrangian formulations are frequently used: formulations based on the Green strain or Almansi strain [1,2] and formulations based on corotational stretch [3,4].

Although velocity strain formulations have been used extensively for nonlinear solids, as exemplified in the work of Key [5], little study has been made of the application of these formulations to structures. Hughes and Liu [6] have presented a formulation based on the global components of the velocity strain.

In this paper, a corotational velocity strain formulation will be presented in which the components of the velocity strain are expressed in a framework that rotates with the material; formulations of this type have been studied by Green and Naghdi [7]. The formulation is then specialized to finite elements

*This work was supported by the Electric Power Research Institute.

by assuming that the rotation within an element is either constant or that the variation in the rotation field is small or moderate.

The potential benefits of these methods are significant. The basic equations are simpler than Green strain or Almansi equations, which endows the resulting computer programs with both simplicity and speed. The stress conjugate to the corotational velocity strain is the Cauchy stress tensor expressed in the corotational system. Any constitutive equations based on Cauchy stress and velocity strain can therefore be used. Furthermore, the corotational stress and stress-strain matrix are both materially objective, so no Jaumann type corrections need be made for the stress state and the formulation is directly applicable to anisotropic materials, which is not true of the formulations given in [5] or [8].

In the next section, the fundamental equations for the corotational velocity strain formulation are presented. Next, the general equations for a finite element application of this formulation is given. In order to illustrate the simplicity of the method, we then give the formulation for a beam element assuming a constant rotation in the element. More complex relations which account for the variation of rotation in an element are then given. The last section gives some examples of the application of this method to nonlinear transient problems.

BASIC EQUATIONS

We will use a kinematical and stress description by Green and Naghdi [7]. Let us denote the material coordinates of the structure by X_i, the spatial coordinates by x_i, the displacements by u_i and the velocities by v_i. Then

$$u_i = x_i - X_i \tag{1}$$

and the deformation gradient F_{ij} is given by

$$F_{ij} = \frac{\partial x_i}{\partial X_j} \tag{2}$$

From the polar decomposition theorem (see [9]) it follows that the deformation gradient can be expressed as a pure deformation, which is expressed by a symmetric matrix U_{kl}, and a rigid body rotation R_{kl} in the form

$$F_{ij} = R_{il}\, U_{lj} \tag{3}$$

The rotation matrix R_{il} is orthogonal, so that

$$R_{il} R_{im} = \delta_{lm} \tag{4}$$

where δ_{lm} is the Kronecker delta.

We will denote the coordinate system which is rotated by the rigid body motion of the material by $\hat{x}_i$ and call it a corotational coordinate system. This system is related to x_i by

$$\hat{x}_i = R_{ij} x_j \tag{5}$$

and its orientation varies from point to point in the material.

The velocity strain (rate of deformation) tensor is given by

$$D_{ij} = \frac{1}{2} \left(\frac{\partial v_i}{\partial x_j} + \frac{\partial v_j}{\partial x_i} \right) \tag{6}$$

and the corotational velocity strain, which is simply the same tensor with its components expressed in the corotational coordinates, is given by

$$\hat{D}_{kl} = R_{ik} R_{j\ell} D_{ij} \tag{7}$$

or

$$\hat{D}_{kl} = \frac{1}{2} \left(\frac{\partial \hat{v}_i}{\partial \hat{x}_j} + \frac{\partial \hat{v}_j}{\partial \hat{x}_i} \right) \tag{8}$$

The state of stress will be represented by the corotational stress $\hat{T}_{ij}$ which are the corotational components of the Cauchy (physical) stress T_{ij}; the two are related by

$$\hat{T}_{kl} = R_{ik} R_{j\ell} T_{ij} \tag{9}$$

The corotational components of the stress are frame invariant, so that the velocity strain is related to the rate of corotational stress by

$$\overset{\circ}{\hat{T}}_{ij} = \hat{C}_{ijkl} \hat{D}_{kl} \tag{10}$$

where the matrix $\hat{C}_{ijkl}$ for a material depends on the state of stress and state variables such as the yield stress but is independent of material rotation, regardless of whether the material is isotropic or anisotropic. This is a key advantage of corotational formulations. If the velocity strain and Cauchy stress are expressed in a fixed coordinate system, a Jaumann rate is required to provide frame invariance, but more importantly, the matrix $\hat{C}_{ijkl}$ must also be modified to account for the rigid body rotation. Furthermore, such formulations are quite awkward in structural theories where it is often convenient to distinguish velocities tangent and normal to the current configuration.

For a material in the domain Ω, the rate of internal work is given by

$$W = \int_{\Omega} D_{ij} T_{ij} \, d\Omega = \int_{\Omega} \hat{D}_{ij} \hat{T}_{ij} \, d\Omega \tag{11}$$

FINITE ELEMENT EQUATIONS

We consider an element which currently occupies a volume Ω^e. Its nodal displacements are u_{iI}, nodal velocities v_{iI} and nodal forces f^{int}_{iI}. We represent the velocities within the element by shape functions

$$\hat{v}_i = N_I (\hat{x}) \hat{v}_{iI} \tag{12}$$

where N_I are the shape functions which are expressed in terms of the corotational coordinates. Throughout this paper, upper case subscripts will refer to nodal values, as exemplified in Eq.(12), and the indicial summation convention will also apply to these subscripts.

The principle of virtual work gives

$$v_{iI}\, f^{int}_{iI} = \int_{\Omega^e} \hat{D}_{ij}\, \hat{T}_{ij}\, d\Omega \tag{13}$$

For elements other than the simplest, i.e. those with linear shape functions, the orientation of the corotational coordinates will vary within the element as shown in Fig. 1. Several alternatives are then available for handling the right hand side of Eq.(13):

i. a single corotational coordinate system $\bar{x}_i$ can be chosen for the element as shown in Fig. 1 and the relative rotations ignored;

ii. a single corotational coordinate system $\bar{x}_i$ can be chosen for the element and the rotations relative to $\bar{x}_i$ can be accounted for by modifying the velocity strain equations;

iii. the relative rotations can be accounted for by using the transformations (7) and (9) at each point of the element.

In this paper we will explore the first and second alternative; the third has been explored by Hughes and Liu [6].

For the first alternative, the use of Eq.(12) gives

$$v_{iI}\, f^{int}_{iI} = \int_{\Omega^e} \bar{v}_{iI}\, \frac{\partial N_I}{\partial \bar{x}_j}\, \bar{T}_{ij}\, d\Omega \tag{14}$$

so the use of the transformation (5) and the arbitrariness of of v_{iI} gives

$$f^{int}_{iI} = R_{ki} \int_{\Omega^e} \frac{\partial N_I}{\partial \bar{x}_j}\, \bar{T}_{kj}\, d\Omega \tag{15}$$

It should be observed that the stress is expressed in terms of a single corotational coordinate system throughout the element. Therefore, if we consider a beam with a constant axial stress $\bar{T}_x$, it follows that the only nonzero nodal forces lie along the $\bar{x}$ axis regardless of the curvature of the beam. This anomaly can yield spurious results whenever the flexural stiffness is small, since it introduces parasitic bending in states of pure membrane stress, cf [10].

The second alternative is to introduce velocity strain relations which account for the variation in rotations of the element but to express their components in the element system. If we represent these relations by

$$\bar{D}_{ij} = D_{ijkI}\,\bar{v}_{kI} \tag{16}$$

then Eq.(15) becomes

$$f^{int}_{iI} = R_{ki}\int_{\Omega^e} D_{mnkI}\,\bar{T}_{mn}\,d\Omega \tag{17}$$

In a subsequent section, forms of Eq.(16) for beams and axisymmetric shells will be presented. Higher order formulations as exemplified by Eq.(17) do provide better accuracy, particularly for relatively coarse meshes, but they do not eliminate parasitic bending.

A SIMPLE BEAM FORMULATION

In order to illustrate the application of a corotational velocity strain, we will first consider a beam element with the simplest corotational formulation where the nodal forces are evaluated by Eq.(15). The notation used is shown in Fig. 2. We will embed the element corotational coordinate within the element so that the $\bar{x}$ - axis always connects nodes 1 and 2. Euler-Bernoulli beam theory will be used, so that the velocities through the depth are completely defined by velocities of the middle surface $V_{\bar{x}}$ and $V_{\bar{y}}$

$$\bar{v}_x = \bar{V}_x - \hat{y}\,\bar{V}_{y,\bar{x}} \tag{18a}$$

so that

$$\bar{D}_x = \frac{\partial \bar{v}_x}{\partial \bar{x}} = \bar{V}_{x,\bar{x}} - \hat{y}\,\bar{V}_{y,\bar{x}\bar{x}} \tag{18b}$$

where commas denote differentiation with respect to the subsequent variables.

The velocity field $\bar{V}_{\bar{x}}$ will be approximated by linear shape functions, and the transverse velocity field of the midline by cubic shape functions so that

$$\bar{V}_x = \xi\,\bar{V}_{x2} \tag{19a}$$

$$\bar{v}_y = \ell(\xi^3 - 2\xi^2 + \xi)\,\phi_1 + \ell(\xi^3 - \xi^2)\,\phi_2 \tag{19b}$$

$$\xi = \bar{x}/\ell \tag{19c}$$

where the rigid body part of the velocity field has been omitted since it causes no strain. The nodal velocities associated with deformation are thus

$$\{\bar{v}\}^T = [\bar{V}_{x2},\ \phi_1,\ \phi_2] \tag{20}$$

and the conjugate nodal forces

$$\{\bar{f}^{int}\} = [f_{x2},\ m_1,\ m_2] \tag{21}$$

where m_I are the nodal moments. Combining Eqs.(18) and (19), we obtain

$$\bar{D}_x = \frac{\bar{V}_{x2}}{\ell} - \frac{\hat{y}}{\ell}\,[(6\xi-4)\phi_1 + (6\xi-2)\phi_2] \tag{22}$$

Equation (15) then gives

$$\begin{Bmatrix} \bar{f}_{x2} \\ m_1 \\ m_2 \end{Bmatrix} = \int_0^1 \int_A \begin{bmatrix} 1 \\ -\hat{y}\,(6\xi-4) \\ -\hat{y}\,(6\xi-2) \end{bmatrix} \bar{T}_x\, dA\, d\xi \tag{23}$$

where A is the cross-sectional area of the beam.

The remaining nodal forces can be obtained from equilibrium

$$\bar{f}_{x1} = -\bar{f}_{x2}$$

$$\bar{f}_{y1} = -\bar{f}_{y2} = \frac{m_1 + m_2}{\ell} \tag{24}$$

HIGHER ORDER VELOCITY STRAIN EXPRESSIONS

The velocity strain expression, Eq.(22), is exact for a beam only when the element's midline is coincident with the $\bar{x}$-axis, which corresponds to the chord between the two nodes. If the beam element is initially curved or if it deforms enough so that the midline displaces substantially from the $\bar{x}$-axis, these equations will be in error because of the following effects:

1. The $\bar{x}$ and $\bar{y}$ axes are no longer coincident with the midline and its normal, respectively, so Eqs.(18) are in error because $\bar{V}_x$ and $\bar{V}_y$ are not along the midline and its normal.
2. The volume integration neglects the deformation of the beam relative to the $\bar{x}$ axis.

In order to account for the first effect without transforming between coordinate systems within the element, higher order velocity strain relations are developed, using the same basic ideas employed in [4] for corotational stretch theories. For this purpose, the displacement of the midline relative to the chord, or $\bar{x}$ axis, is denoted by Y. It will be assumed that

$$\frac{Y}{\ell} = O(e) \qquad \bar{Y}_{,\bar{x}} = O(e) \qquad Y_{,\bar{x}\bar{x}} = O(e^2) \qquad Y_{,\bar{x}} = Y_{,\hat{x}} \tag{25}$$

and accuracy of order e^2 is assumed; terms of higher order and certain other terms are neglected. Because of space limitations, we omit the derivation, and give only the final result

$$\bar{D}_x = d_1 - \hat{y}\kappa_1 \tag{26a}$$

$$d_1 = \bar{V}_{x,\bar{x}} + Y_{,x}\,\bar{V}_{y,\bar{x}} \tag{26b}$$

$$\kappa_1 = (1 - \tfrac{1}{2} Y_{,\bar{x}}^2)\,\bar{V}_{y,\bar{x}\bar{x}} + \underline{Y_{,\bar{x}\bar{x}}\,\bar{V}_{x,x}} \tag{26c}$$

For an axisymmetric shell element, we let x correspond to the radial coordinate, r, and θ be the circumferential coordinate. The corresponding relations are

$$\bar{D}_x = d_1 - \hat{y}\kappa_1 \tag{27a}$$

$$\bar{D}_\theta = d_z - \hat{y}\kappa_2 \tag{27b}$$

where $\bar{D}_\theta$ is the hoop velocity strain. The terms d_1 and κ_1 are identical to those for the beam, Eqs.(26), while

$$d_2 = \frac{V_x}{r} = \frac{1}{r}\,(\bar{V}_x \cos\alpha + \bar{V}_y \sin\alpha) \tag{28a}$$

$$\kappa_2 = \frac{1}{r} Y_{,x}\, \bar{V}_{x,\bar{x}} \cos\alpha + \underbrace{\frac{1}{r}\,[r(\cos\alpha - Y_{,x}\sin\alpha) - Y\sin\alpha\cos\alpha]V_{y,\bar{x}}} \tag{28b}$$

where r is the current radial coordinate of a point, α the current angle between $\bar{x}$ and x, as shown in Fig. 2. For all applications we have considered so far, the second terms in the expressions for κ_1 and κ_2 have been insignificant.

EXAMPLES

Results are given for a clamped ring shown in Fig. 3, for which experimental results are reported in [11]; numerical results have been reported in [3]. Explicit time integration with the central difference method and a lumped mass matrix was used. The material model is elastic-plastic with a Mises yield condition and isotropic hardening. Because the width of the ring is large compared to its thickness, plane strain was assumed in the z-direction. Furthermore, the compressibility of the elastic strains was considered neglible, so the height h of the cross-section was modified by

$$h = h_o \ell_o / \ell \tag{29}$$

for both the velocity strain computations, Eq.(18b), and the nodal force computtations, Eq.(23). The nodal forces were obtained by numerical quadrature using five points through the thickness, and two points along the length with a trapezoidal rule.

The displacements for the midpoint of the clamped ring are compared for plane stress and plane strain, with and without the area correction of Eq.(29), in Table 1. As can be seen, the effects of the plane strain assumption are very significant, changing the result by 20%. The effect of the thickness correction is less pronounced but nevertheless not neglible.

TABLE 1

EFFECTS OF ASSUMPTIONS ON MIDPOINT DEFLECTION OF CLAMPED RING

Assumptions	Midpoint deflection (in)
Plane strain, variable thickness	2.99
Plane strain, constant thickness	3.06
Plane stress, variable thickness	3.43
Plane stress, constant thickness	3.53

The plane strain solution with thickness correction compares best with the experiment, so we will restrict all subsequent comparisons to this case. The time history of the midpoint is compared to the experiment in Fig. 4. The reported experimental results exhibit considerable snapback, which are absent in the computations. Figures 5 and 6 compare the deformed shape and strain time histories with the experiment. Overall, the agreement is quite good and comparable to that of the numerical results reported in [3].

REFERENCES

1. K.J. Bathe and H. Ozdemir, "Elastic-Plastic Large Deformation Static and Dynamic Analysis," Computers and Structures, Vol. 6, 1976, pp. 81-92.

2. S. Yaghmai and E.P. Popov, "Incremental Analysis of Large Deflections of Shells of Revolution," International Journal of Solid and Structures, Vol. 7, 1971, pp. 1375-1393.

3. T. Belytschko and B.J. Hsieh, "Nonlinear Transient Finite Element Analysis with Convected Coordinates," International Journal for Numerical Methods in Engineering, Vol. 7, 1973, pp. 255-271.

4. T. Belytschko and L.W. Glaum, "Applications of Higher Order Corotational Stretch Theories to Nonlinear Finite Element Analysis," Computers and Structures, Vol. 10, 1979, pp. 175-182.

5. S.W. Key, "HONDO - A Finite Element Computer Program for the Large Deformation Dynamic Response of Axisymmetric Solids," Report SLA-74-0039, Sandia Laboratories, April 1974.

6. T.J.R. Hughes, and Y.K. Liu, "Nonlinear Finite Element Analysis of Shells - Part I, Three Dimensional Shells," to be published Computer Methods in Applied Mechanics and Engineering.

7. A.E. Green and P.M. Naghdi, "A General Theory of an Elastic-Plastic Continuum," Archives of Rational Mechanics and Analysis, Vol. 18, 1965, pp. 251-281.

8. M.L. Wilkins, "Calculation of Elastic-Plastic Flow," Report UCRL-7322-Revision 1, Lawrence Radiation Laboratory, University of California, Livermore, 1969.

9. L. Malvern, Introduction to the Mechanics of a Continuous Medium, Prentice-Hall Incorporated, Englewood Cliffs, New Jersey, 1969.

10. T. Belytschko, "Nonlinear Analysis - Descriptions and Numerical Stability," in Shock and Vibration Computer Programs, edited by W. Pilkey and B. Pilkey, The Shock and Vibration Information Center, 1975, pp. 537-562.

11. H.A. Balmer and E.A. Witmer, "Theoretical-Experimental Correlation of Large Dynamic and Permanent Deformation of Impulsively Loaded Simple Structures," Report FDL-TDR-64-108, Air Force Flight Dyn. Lab., Wright-Patterson Air Force Base, Ohio, 1964.

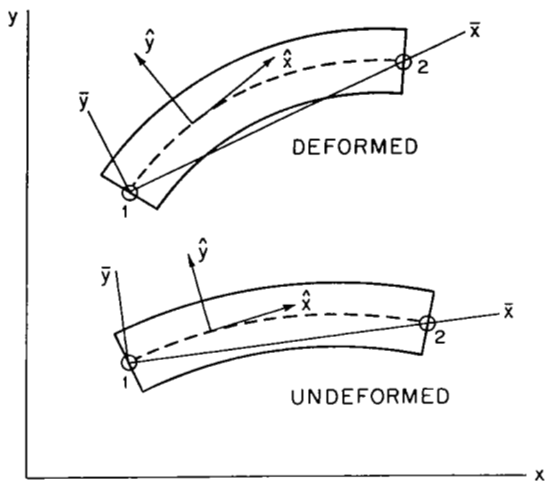

Fig. 1. Deformed and undeformed beam element showing element corotational coordinates $\bar{x},\bar{y}$ and local corotational coordinates $\hat{x},\hat{y}$.

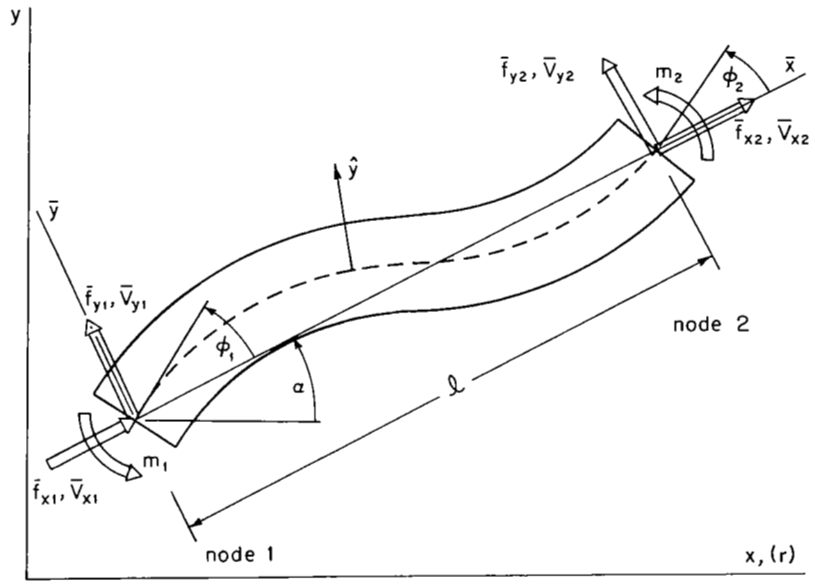

Fig. 2. Nomenclature for nodal forces and velocities.

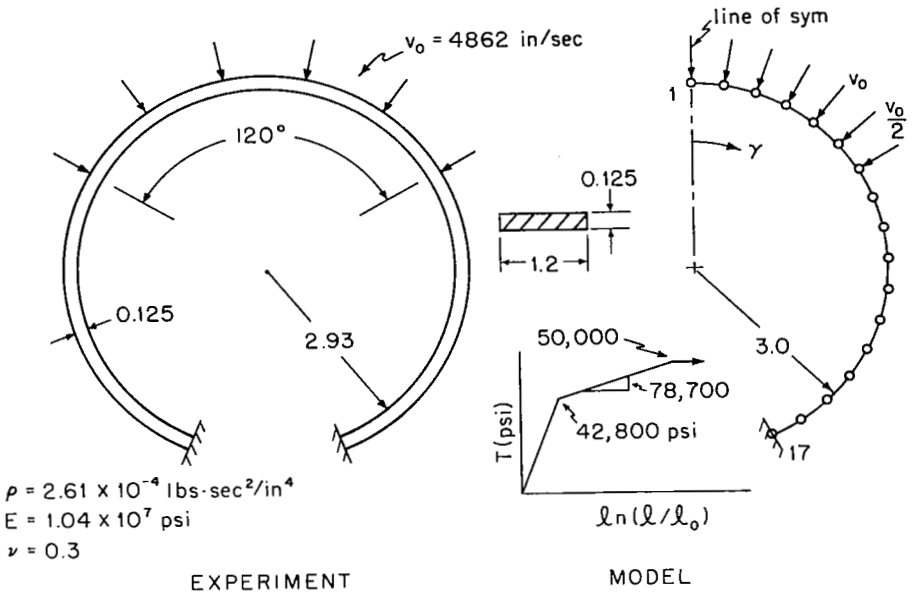

Fig. 3. Experiment [11] and model for clamped ring problem.

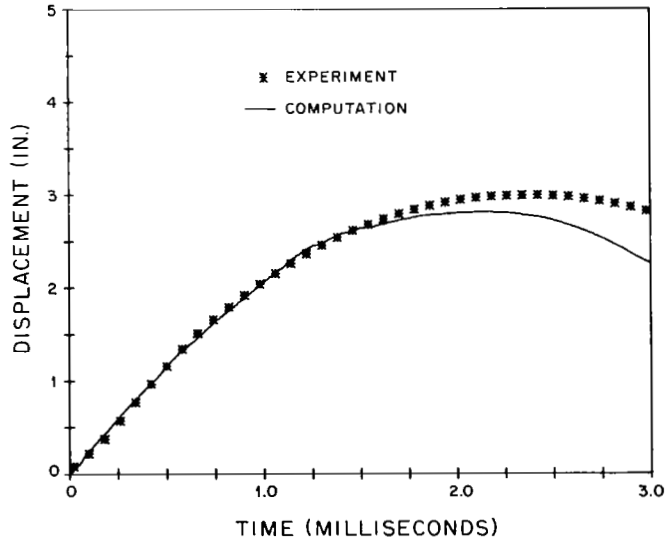

Fig. 4. Comparison of computed centerpoint (node 1 in Fig.3) vertical displacement with experimental results [11].

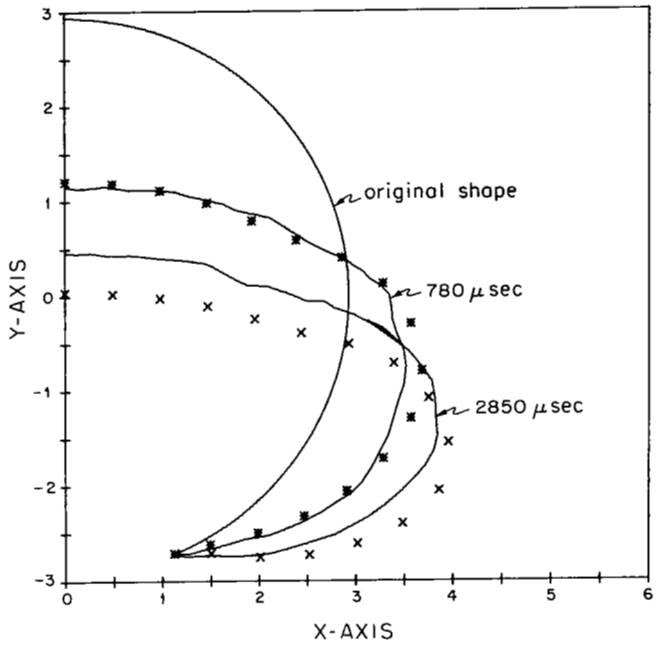

Fig. 5. Deformed configuration of clamped ring compared to experimental results [11].

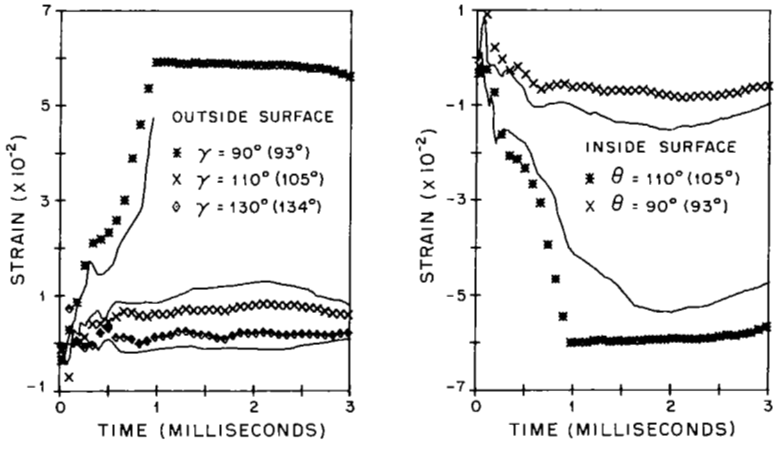

Fig. 6. Comparison of computed strains against experimental results [11]; angle in parenthesis is for the experimental record.